Advanced Powder Technology 33 (2022) 103635

Contents lists available at ScienceDirect

Advanced Powder Technology

journal homepage: www.elsevier.com/locate/apt

Original Research Paper

A computational approach to understand the breathing dynamics and pharmaceutical aerosol transport in a realistic airways

Akbar Arsalanloo [a], Majid Abbasalizadeh [a,*], Morteza Khalilian [a], Yalda Saniee [b], Ahad Ramezanpour [c], Mohammad S. Islam [d]

[a] Department of Mechanical Engineering, Faculty of Engineering, Urmia University, Urmia, Iran
[b] Department of Medical Diagnostic Imaging, Urmia University of Medical Sciences, Urmia, Iran
[c] School of Engineering and the Built Environment, Anglia Ruskin University (ARU), Bishop Hall Lane, Chelmsford, Essex, UK
[d] School of Mechanical and Mechatronic Engineering, University of Technology Sydney, Ultimo, NSW 2007, Australia

ARTICLE INFO

Article history:
Received 2 April 2022
Received in revised form 22 April 2022
Accepted 19 May 2022
Available online 3 June 2022

Keywords:
Targeted drug delivery
Realistic model of respiratory airways
Discrete Phase Model (DPM)
Particle deposition
Eulerian-Lagrangian method

ABSTRACT

Targeted drug delivery is an advanced method discussed in the literature for optimized treatment of diseases. However, the data for a precise understanding of pharmaceutical aerosol transport to the desired positions in the airways is not sufficient in the literature. Hence, in this work the transport and deposition of particles have been studied numerically in a realistic model of the respiratory system. The model was reconstructed based on CT-scan images of a healthy 28-year-old male and the commercial code ANSYS Fluent was used for analysis. After validation, distribution and deposition patterns of particles have been presented along with analysis of flow field dynamics. It was found that majority of particles enter the right lung while deposition is higher in the left lung and that the left lower lobe, left upper lobe and right lower lobe have the highest rate of lobar deposition. It was also observed that inertial impaction plays the dominant role in deposition of larger diameter particles at higher flow rates at the upper airways. The present findings improve our insight toward regional distribution and deposition of particles and assists in more accurate prediction of particle transport for drug delivery.

1. Introduction

Millions of people are dealing with respiratory system health issues such as cancer and asthma all over the world. Drug delivery via the respiratory system is a conventional method for treating diseases [1–3]. However, delivery of drugs to body by inhaling pharmaceutical aerosols may expose the whole respiratory system to medications and cause unwanted side effects. The shortage of conventional methods urges scientists to adopt more efficient solutions for delivering drugs to specific locations and avoid collateral damage [4–6]. Targeted delivery of drugs remarkably optimizes efficiency of cures by exposing only the desired regions to medications however, studying on this issue needs contributions from other areas of expertise according to the interdisciplinary nature of respiration.

For targeted drug delivery, scientists should have a thorough understanding about characteristics of air flow in different regions of respiratory system along with distribution and deposition patterns of pharmaceutical aerosols [7,8]. As real process of respiration is so complicated and it is impossible to simulate all features of respiration in just one study, most numerical studies are based on simplified assumptions to reduce computational costs and make it possible to concentrate on more desired features of respiration [9]. Idealized geometry, steady state flow assumption, rigid wall surfaces and fixed position assumption for airways without counting for motion of lungs in the analysis are the most common simplifications utilized in the literature. Additionally, some researchers have omitted several parts of the whole respiratory system in their investigations in order to accurately capture the phenomenon which has the higher priority in the intended regions.

Islam et al. studied spherical and non-spherical particle transport and deposition in different geometries of respiratory airways [10]. In another study, in order to unfold effect of turbulence and geometric characteristics on the transport and deposition of polydisperse particles in the upper airways, Islam et al. [11] adopted different anatomical models in both turbulent and laminar flows.

To generate the model for CFD calculations, experts have used image processing techniques to rebuild realistic 3D models based on complex geometries of upper and lower respiratory airways.

* Corresponding author.
E-mail address: m.abbasalizadeh@urmia.ac.ir (M. Abbasalizadeh).

https://doi.org/10.1016/j.apt.2022.103635

Nomenclature

Symbols

ρ	fluid density [kg/m^3]
ρ_P	density of particles [kg/m^3]
μ	dynamic viscosity of air [kg/m-s]
τ_D	particle relaxation time [s]
u	fluid velocity [m/s]
u_P	particle velocity [m/s]
t	time [s]
C_D	particle drag coefficient
Re_r	relative Reynolds number
t_s	characteristic time scale of fluid [s]
d_P	particle diameter [μ m]
L_S	flow characteristic length [m]
V_S	flow characteristic velocity [m/s]
Q	air flow rate [lpm]
St	stokes number
g	gravitational acceleration [m/s^2]

Acronyms

DPM	Discrete Phase Model
DE	Deposition Efficiency
DF	Distribution Fraction
LPM	Liter Per Minute
RANS	Reynolds-Averaged Navier-Stokes
SIMPLE	Semi-Implicit Method for Pressure Linked Equations
EWT	Enhanced Wall Treatment
RSM	Reynolds Stress Model
DNS	Direct Numerical Simulation
LES	Large Eddy Simulation
DICOM	Digital Imaging and Communications in Medicine
CT-Scan	Computed Tomography Scan

Gu et al. [12] studied effect of structural modifications made to the tracheobronchial tree after the lobectomy. Gosh et al. [13] used magnetic to enhance targeted delivery of drugs to a specific location in the airways.

Sigh et al. [14] numerically studied effect of airway stenosis on the air flow field and particle deposition and transport at lower airways. Effect of expansion and contradiction of lungs is not considered in most previous works. Hunter et al. [15] investigated effect of moving wall up to the third generation of respiratory airways in an idealized geometry. Using CFD techniques, experts can evaluate flow field conditions in diseased lungs. Sul et al. [16] and Chen et al. [17] numerically studied flow field in an obstructed airway and compared it with a healthy one. Koullapis et al. [18] verified effect of velocity profile and flowrate and electrostatic charge carried by discrete phase on deposition of particles. Main purpose for studying flow field and particle deposition in the airways is to optimize delivery of drugs to particular locations. One practical method suggested in the literature for conducting the particles inside airways is to impose external magnetic field [19]. Zhao et al. [20] conducted a numerical study to analyze effect of carrier shape on the dispersion and deposition of particles from a dry powder inhaler. Effect of respiratory flow rates is studied in the work of Rahimi Gorji et al [21]. Phuong et al. [22] performed computational study on convective heat transfer in the whole respiratory airways including the oral and nasal cavity to the end of the trachea in both steady and unsteady breathing conditions. Narayanan et al. [23] verified effect of inlet temperature on the flow field and particle deposition in a highly idealized mouth throat model. Soni and Aliabadi [24] simulated airflow and deposition of particles in an idealized ten generation model of bronchial tubes. Deng et al. [25] performed a numerical study on deposition of particles in three age groups: a 7 months infant, 4 year old child and a 20 year old adult man. Comparison of the results showed that the deposition rate for infants and children is higher than adults. One major outcome of this study was that unlike adults, particles deposit mainly in the upper airways for infants. Li et al. [26] and Shang et al. [27] added outside breathing zone to the computational domain to evaluate how surrounding atmosphere affects flow patterns and particle deposition in airways. Koullapis et al. [28] conducted a comprehensive numerical-experimental study to explain the flow field and two-phase flow characteristics in different regions of upper and lower airways. Rahman et al. [29] studied the aging effects on particle transport deposition in lungs of people in age of 50–70 and reported that 100% of the particles with diameter of 20 μm get deposited at upper airways. In another recent study, Rahman et al. [30] numerically studied particle transport and deposition in realistic model with and without stenosis. Sommerfeld et al. [31] analyzed flow field and particle deposition in the lower respiratory airways for different particles with different diameter and reported regional deposition and flow filed patterns. Williams et al. [32] carried out a numerical study on a realistic model of airways with considering different breathing profiles and taking into account effect of particle-particle interaction on the deposition efficiency. Kim et al. [33] numerically studied performance of a newly designed dry powder inhaled in terms of particle deposition in different regions of respiratory airways. In this study, CFD was coupled with DEM to evaluate the functionality of this device. CFD methods has shown to be an important asset for providing deeper insight towards diseases of pulmonary system. Chen et al. [34] used an idealized geometry with two consecutive bifurcations to study effect of asthma on the airflow dynamics and particle deposition in the bifurcations. In another study, Tohidi et al. [35] investigated effect of nasal airway obstruction in the dispersion and deposition of particles in the nasal airways in a realistic model. In a most recent study, Liu et al. [36] generated realistic model based on a child upper airway to study transport and deposition of particles in the nasal and upper air ways. Wu et al. [37] used a magnetic drug targeting method to deliver pharmaceutical particulates to a desired region in the left lung in a model based on real respiratory system. Xu et al. [38] verified effect of ambient temperature and humidity on particle growth and deposition and distribution in a realistic model of upper and lower respiratory airways.

So far, many studies have been conducted to unfold all mechanical features of respiration and deposition of particles in lungs however, the patient specific nature of the respiratory airways and differences in individual morphological shape of the respiratory system and the importance of understanding flow details in respiratory airways has biased the researchers to dedicate extra effort to study air flow dynamics and particle distribution and deposition in both the upper and lower respiratory airways. Hence, in this work a great effort has been made to study features of two-phase flow in the lower respiratory airways based on a patient specific realistic model human respiratory system. Different breathing conditions and different particle sizes have been considered in this work to better evaluate the realistic conditions. The

flow field characteristics, distribution and deposition of particles in a realistic model of respiratory airways including the main trachea, main stem bronchi, lobar and segmental bronchi have been studied and analyzed. The model is reconstructed based on CT-scan images of a healthy non-smoking adult male with no problems in his respiratory system. The results have been presented in terms of velocity profile and velocity contours, distribution fraction and deposition efficiency of particles along with deposition patterns of particles in different regions of the airways. This study also presents a comparison of particle distribution among different lungs and lobes of the respiratory system.

2. Numerical method

2.1. Anatomy of respiratory system

Respiratory system is one of the most vital organs in human body which is responsible for supplying the oxygen needed for body and removing the produced carbon dioxide. The air we breathe enters the nasal cavity and is conducted through the airway passages until it ends up some bubble shaped air sacs called the alveoli, where oxygen-carbon dioxide exchange takes place and the carbon dioxide escapes human body through the same passages.

The respiratory system can be divided into two main regions, the upper respiratory system and the lower respiratory system. Upper respiratory system consists of nasal cavity, pharynx and larynx. The upper respiratory airway passages warm and clean the air and conduct it toward the lower respiratory airway passages. Lower respiratory system consists of the trachea, bronchi and the alveoli. Below the larynx is trachea which conducts the air to the lungs. Trachea at its end divides into two main bronchi which are the main branches for the right and left lungs. These are called main bronchi or primary bronchi. Each of the main bronchus subdivides further to smaller branches that conduct air to different lobes of lungs. These secondary bifurcations are called lobar bronchi or secondary bronchi. The right lung has three lobes called the upper lobe, middle lobe and the lower lobe while the left lung as a reason of presence of heart has only two, the upper lobe and the lower lobe. Each of these lobes again subdivides into smaller segments that comprise the third generation of airway passages called segmental or tertiary bronchi. There are total of ten segmental bronchi at each lung. The air passes through 23 generations of airways before it reaches the alveoli where blood cells exchange carbon dioxide with oxygen.

In this work we have simulated the airflow and deposition of particles inside the respiratory tract. Our simulation includes the main trachea along with main, lobar and segmental bronchi for both the right and left lungs. Fig. 1 depicts structure of the respiratory airways simulated in this work with names and positions of different lobes and segments. The morphological characteristics of different sections demonstrated in Fig. 1, including the perimeter and hydraulic dimeter have been presented in Table 1 [39].

2.2. Geometry and meshing

We have used CT-Scan (Computed Tomography Scan) images of an adult non-smoking male with no problems in his respiratory system to reconstruct a realistic 3d model of the tracheobronchial tree. 266 images in DICOM format with the following specifications were used to build the 3d model: 0.8 mm slice thickness, 512*512 spatial resolution, 35 cm field of view (FOV), 120 kV, 250 mA. DICOM is a conventional format for transmitting medical images and data and is supported by most of the medical imaging systems. These images were imported to 3D-Doctor for generating the geometry. 3D-Doctor is an advanced 3d modeling and image processing software for medical applications. After segmenting the airway passages at each slice under supervision of a radiology expert, the 3d model was reconstructed and smoothed by the software. The model with STL format was exported to ANSYS ICEM to be prepared for simulations. Fig. 2 shows the segmented airway in one slice and the whole generated 3d model in 3D-Doctor.

In ANSYS ICEM, the outlets were extended further downstream to avoid reversed flow at the outlet sections. In order to have regional deposition reports, the model was separated at each of the lobar and segmental bronchus to have distinct walls for different regions of the respiratory system. According to the complicated geometry of respiratory airways, unstructured mesh with tetrahedral elements was generated along with five prismatic layers at the boundary layer region adjacent to the wall. As near wall fluctuations affect the trajectory of particles in this region, in order to accurately model the trajectories and deposition of particles, the prismatic boundary layer cells were generated to properly capture near wall turbulence. The final model generated and different views of the generated mesh are depicted in Figs. 3 and Fig. 4.

2.3. Continuous phase

in the literature, three major methods have been used to simulate airflow and calculate deposition of particles in the respiratory airways which are the direct numerical simulation (DNS), large eddy simulation (LES) and Reynolds-averaged Navier-Stokes (RANS) turbulent models. DNS is a computational method that resolves all the range of temporal and spatial scales of the turbulent flow and there is no turbulence modeling in this method. Resolving the entire range of turbulent scales makes DNS computationally expensive such that it is not efficient to apply this method to most of the practical engineering problems. There are few researches performed on respiratory airways using direct numerical simulation as a reason of high computational costs. Lin et al. [40] used DNS to investigate effect of laryngeal jet on the airflow in the intra-thoracic airways and Fotos et al. [41] also used an idealized model to study airflow and particle deposition in a single airway bifurcation. LES however, filters eddies in small scales and uses turbulent modeling for them while large eddies are directly resolved similar to DNS method. Although LES is computationally less expensive in comparison with DNS, it still needs great computational facilities. RANS uses time-averaged Navier-Stokes equations to model the turbulence fluctuations and consumes less computational costs in comparison with the last two methods. In this work, the Reynolds Stress Model (RSM) turbulence model has been used to properly capture the flow features. For adequate modeling of the near wall region the Enhanced Wall Treatment has been adopted to better capture the near wall parameters. In RSM, six extra transport equations are solved for the Reynolds stresses and one other transport equation for the dissipation rate. Generally, RSM is better for resolving the intense anisotropy of the turbulence in flows with anisotropy nature including reversed flows and secondary vortices. Accuracy and proficiency of RSM model has also been previously reported in the literature in the work of sommerfeld et al. [31]. For the EWT model to act properly, the dimensionless distance from the wall for the first cell centroid should be on the order of one (y^+ 1) as recommended by the ANSYS Fluent user's guide [42]. In this work the height of first cell is 0.08 mm to ensure the requirements need for y^+.

The continuous phase which is air in this work, has been simulated using Eulerian method and was assumed to be incompressible and Newtonian with density of ρ = 914 kg/m^3 and dynamic viscosity of μ = 1.8e-05 Pa.s and the flow was assumed to be in steady state. Although the nature of breathing is unsteady, however the steady flow assumption can properly predict flow field

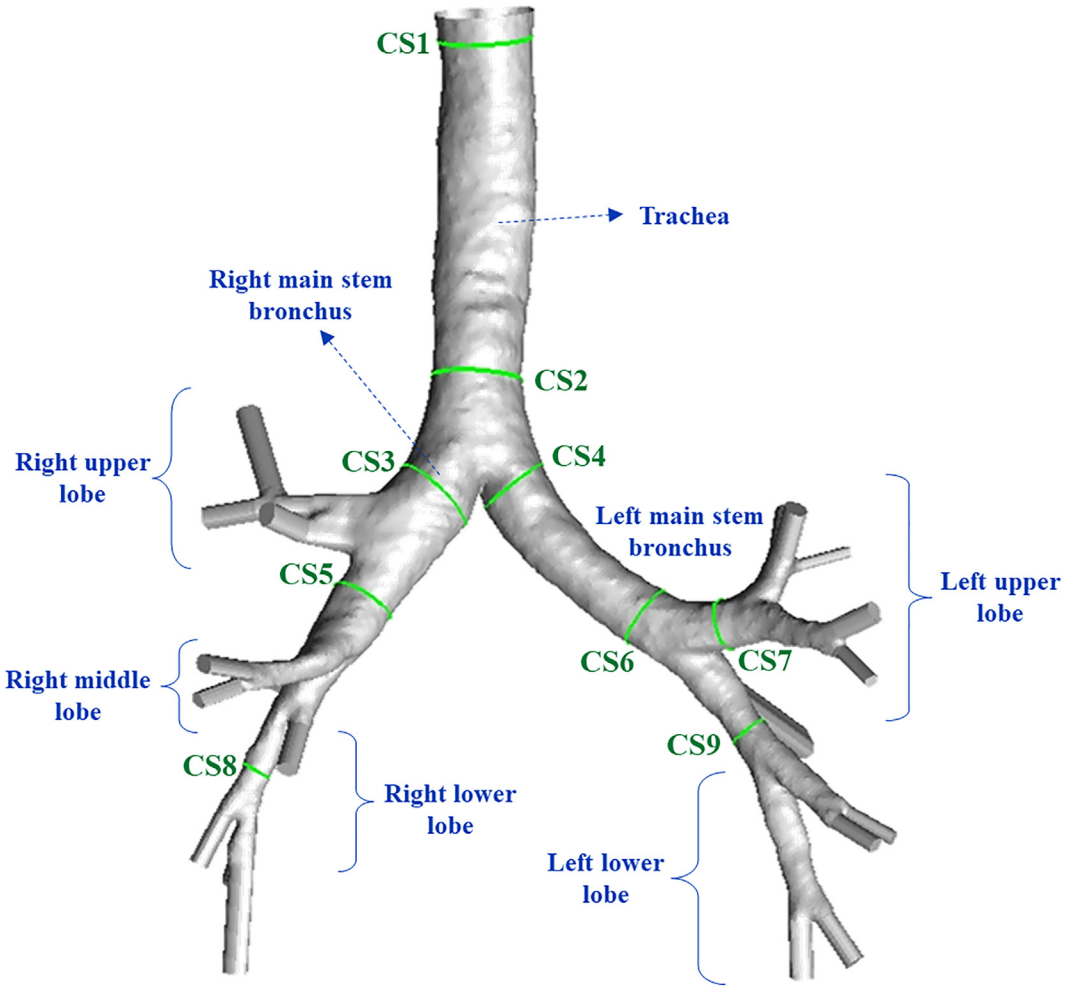

Fig. 1. Anatomy of respiratory system simulated in this study along with names of different regions. The perimeter and hydraulic diameter of the different cross sections indicated in this figure have been presented in Table 1.

Table 1
Morphological characteristics of the model at different sections of different bronchi.

	Position of the slice	Perimeter (P)	Hydraulic diameter (d_h)
CS1	**Trachea (beginning)**	**55.11 mm**	**16.38 mm**
CS2	**Trachea (end)**	**51.85 mm**	**16.01 mm**
CS3	**Right main stem bronchus**	**46.93 mm**	**14.23 mm**
CS4	**Left main stem bronchus (beginning)**	**41.54 mm**	**12.74 mm**
CS5	**Right intermediate bronchus**	**34.09 mm**	**10.54 mm**
CS6	**Left main stem bronchus (end)**	**34.72 mm**	**10.71 mm**
CS7	**Left upper lobe**	**29.52 mm**	**9.18 mm**
CS8	**Right lower lobe**	**18.1 mm**	**5.71 mm**
CS9	**Left lower lobe**	**22.36 mm**	**6.83 mm**

in the realistic unsteady breathing except in the deceleration phase and when there is flow reversal. Hence, steady flow assumption has been prevalently made in the literature [43,44]. As we have no heat transfer in this work, the energy equation was not solved in the analysis. SIMPLE method was used for pressure-velocity coupling and the second order upwind was used as the discretization method. We assumed the problem to be converged when the residuals were reduced below 10e-5 except for the continuum equation that the amount of 10e-04 was assumed to suffice as the convergence criteria.

Three flow rates of 15 L/m, 30 L/m and 60 L/m have been used in this work which are respectively associated to sedentary, light and heavy breathing conditions [45]. For inflow boundary conditions, mass flow inlet was used and pressure outlet condition was applied for the outlets. Moreover, the walls were assumed rigid and no slip boundary condition was applied at the walls.

2.4. Discrete phase

A Eulerian-Lagrangian approach is used to simulate the trajectories and deposition of particles in the fluid flow. In Discrete Phase Model (DPM), the continuous phase flow field is obtained using RANS models and after the solution was converged, the particles are released in the computational domain and trajectories of particles are calculated. The particles have been injected from a surface which is at the upstream of the inlet to allow the particles disperse properly before reaching the main trachea. Initial velocity of the particles has been set to be equal to the inlet velocity of the air flow. It is to be noted that in DPM which calculates trajectories of particles in Lagrangian frame of reference, particles are not treated as a continuous phase and no transport equation is solved for them as it was done for the continuous phase, instead for each particle, the equation of motion is solved to achieve its trajectory. This equation is written as [46]:

$$\frac{du_p}{dt} = F_D \times (u - u_p) + \frac{g(\rho_p - \rho)}{\rho_p} + F \quad (1)$$

Where.

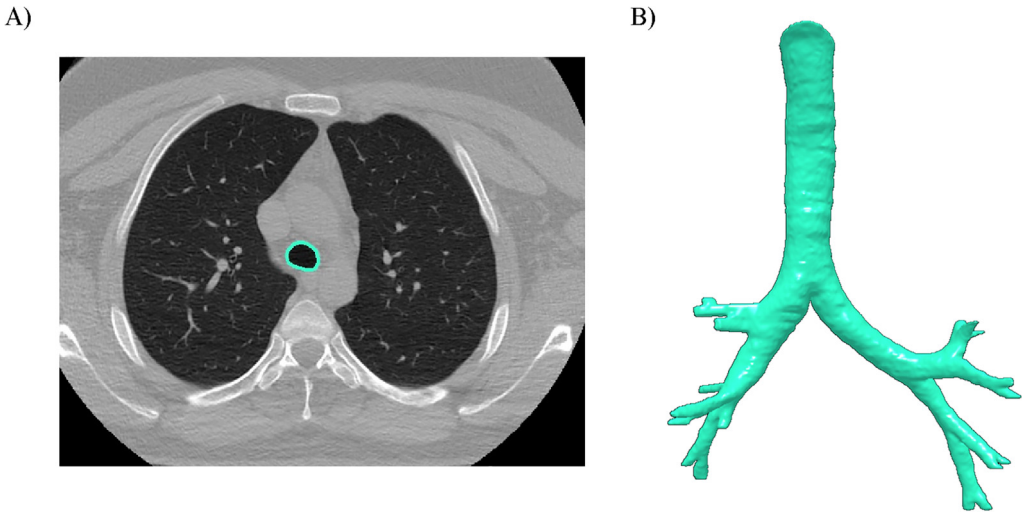

Fig. 2. Reconstruction of 3D model. A) Segmented airway in one.

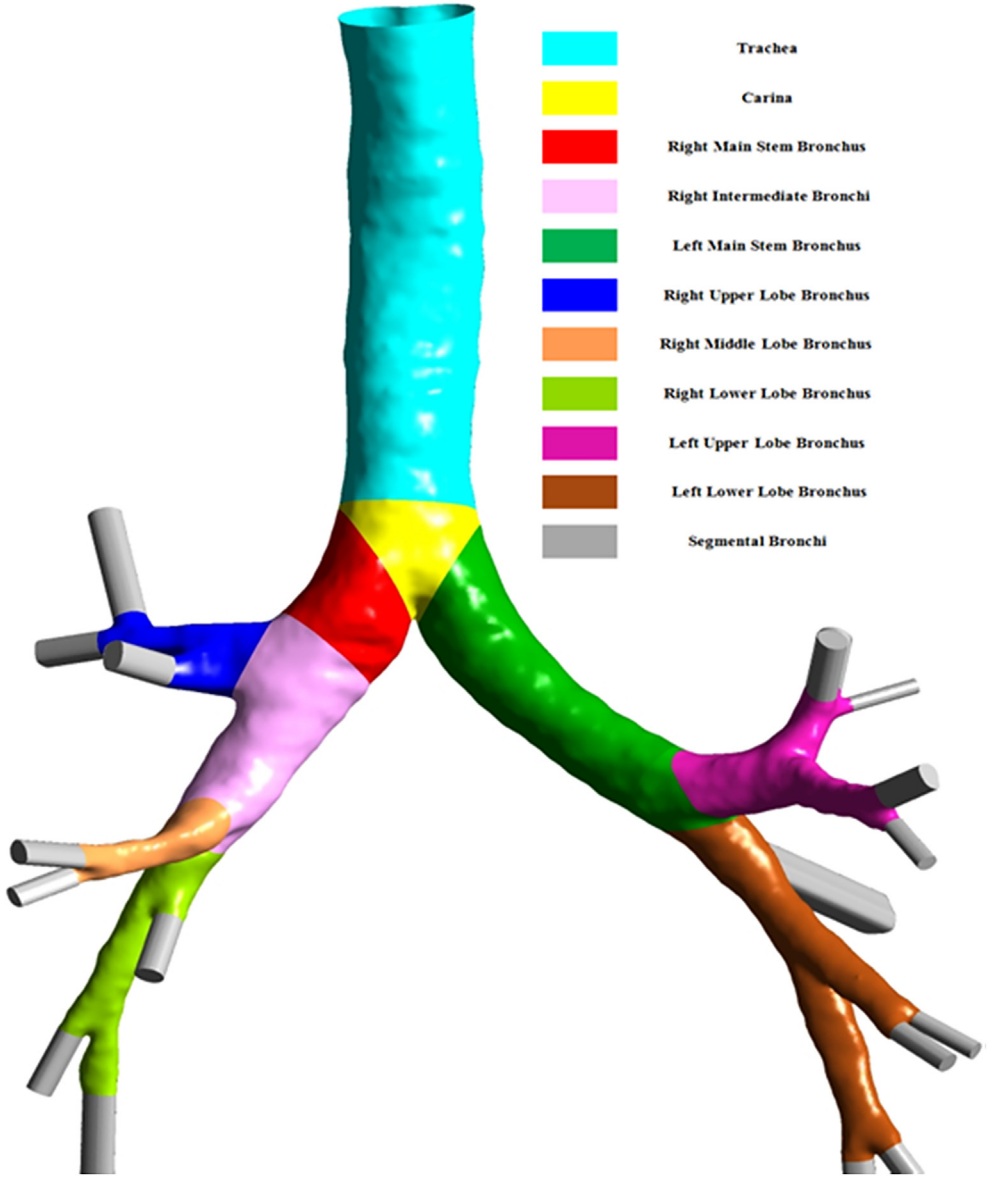

Fig. 3. Final model with extended outlets.

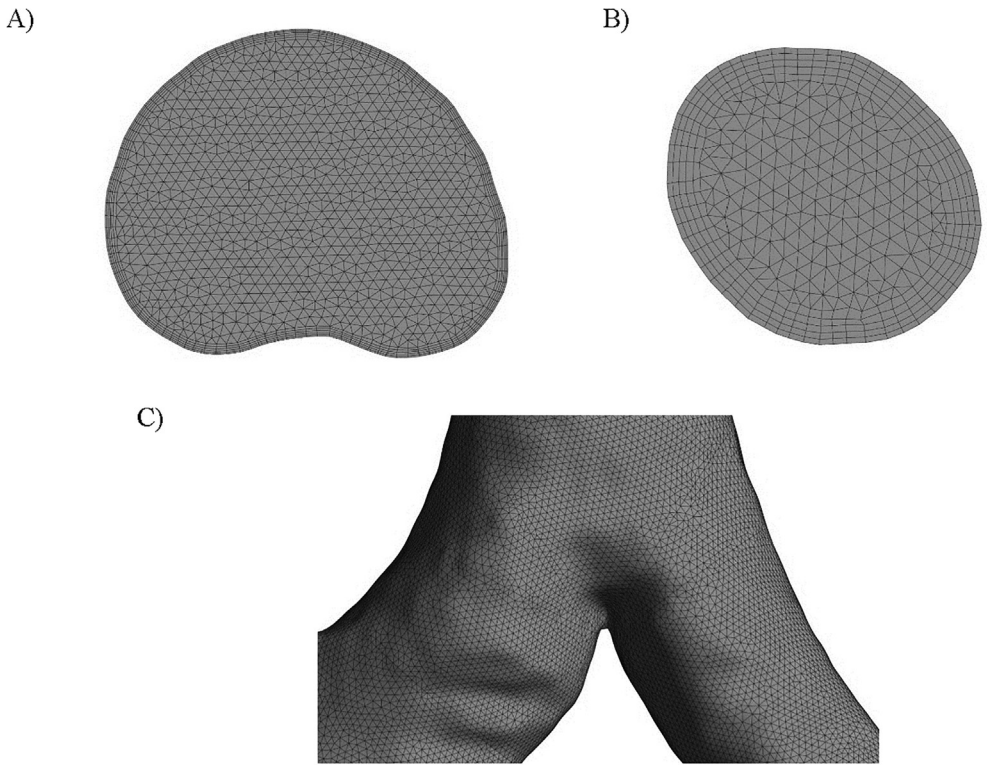

Fig. 4. Different views of generated mesh. A) Inlet, B) Outlet of the apical segmental bronchi at right upper lobe, C) Anterior view of the model with generated grids.

$$F_D = \frac{18\mu}{\rho_p {d_p}^2}\frac{C_D Re_r}{24} \tag{2}$$

And

$$Re_r = \frac{\rho d_p |u_p - u|}{\mu} \tag{3}$$

Eq. (1) equates rate of change in inertia of particles with the forces acting on them. It is to be mentioned that Eq. (1) is written for a unit particle mass. The first term on the right side is drag force and the second term on the right side is Buoyancy force which is defined as the force exerted to a particle immersed in a fluid. In the equations above, u_p, ρ_p, d_p respectively stand for velocity, density and diameter of particles and u, ρ, μ stand for velocity, density and dynamic viscosity of air. C_D is the drag coefficient which is written as [47]:

$$C_d = \frac{24}{Re_r} \tag{4}$$

For $Re_r < 1$ and for $1 < Re_r < 400$, C_D is defined as:

$$C_D = \frac{24}{Re_r}\left(1 + 0.15{Re_r}^{0.687}\right) \tag{5}$$

The particles are assumed spherical and spherical drag law is applied for them. In Eq. (1), F represents additional forces that might affect motion of particles in particular circumstances. These forces could be thermophoretic force, Brownian force, virtual mass force and Saffman's lift force. As there is no temperature gradient, there is no thermophoretic force either. Brownian force is important in laminar flow and for sub-micron particles which is not true about this simulation. Virtual mass force plays an important role when density of the carrier phase is much greater than density of the discrete phase ($\frac{\rho}{\rho_p} \gg 1$), however it is not true in this work which is why the virtual mass force is assumed to be negligible. Saffman's lift force is a lift force upon the particles due to shear and is significant for sub-micron particles. As the diameter of particles in this work range from 1 μm to 14 μm, this force is not included in the equation of motion. Accordingly, the only forces that are important in Eq. (1) are the buoyancy and drag and all additional forces are negligible.

The particles are injected into the domain from the inlet surface. The boundary conditions of DPM for outlets are set to "escape" and as there is no bounce of particles from the surface, the boundary condition of the discrete phase for walls is set to "trap". The deposition takes place when the distance between particle center and the wall is less than radius of particle and in such circumstance the software reports fate of particle as trapped. Deposition efficiency of particles for each region is defined as number of particles deposited in that region to the total number of particles that have entered the computational domain.

2.5. Grid refinement results

In order to assure the accuracy of numerical results, the grid independence analysis should be carried out before the main analysis to find the optimum case in which the results do not change significantly by further refinement of grid. In this work, two different methods have been used to check the computational domain for the best grid which are the velocity profiles and the total deposition rate of particles with three different diameters of 2.5, 6 and 10 μm. Fig. 5 depicts the grid refinement results based on the velocity profiles (Fig. 5 C,D,E) on different sections (as shown in Fig. 5B) and total deposition efficiency of particles (Fig. 5A). Fig. 5 implies that the results do not vary significantly by increasing the number of elements from 1,323,000 to 1765000. It is to be noted that although the velocity profiles of grids with 918,000 and 1,323,000 elements are rather identical, but in some points there are slight differences between their velocity profiles while in Fig. 5A it is observed that there is some difference between the deposition efficiency of the grid with 918,000 and 1,323,000 elements. Hence, for higher accuracy and higher mesh quality, the grid with 1,323,000 elements has been selected for rest of the study. The grid elements have been generated

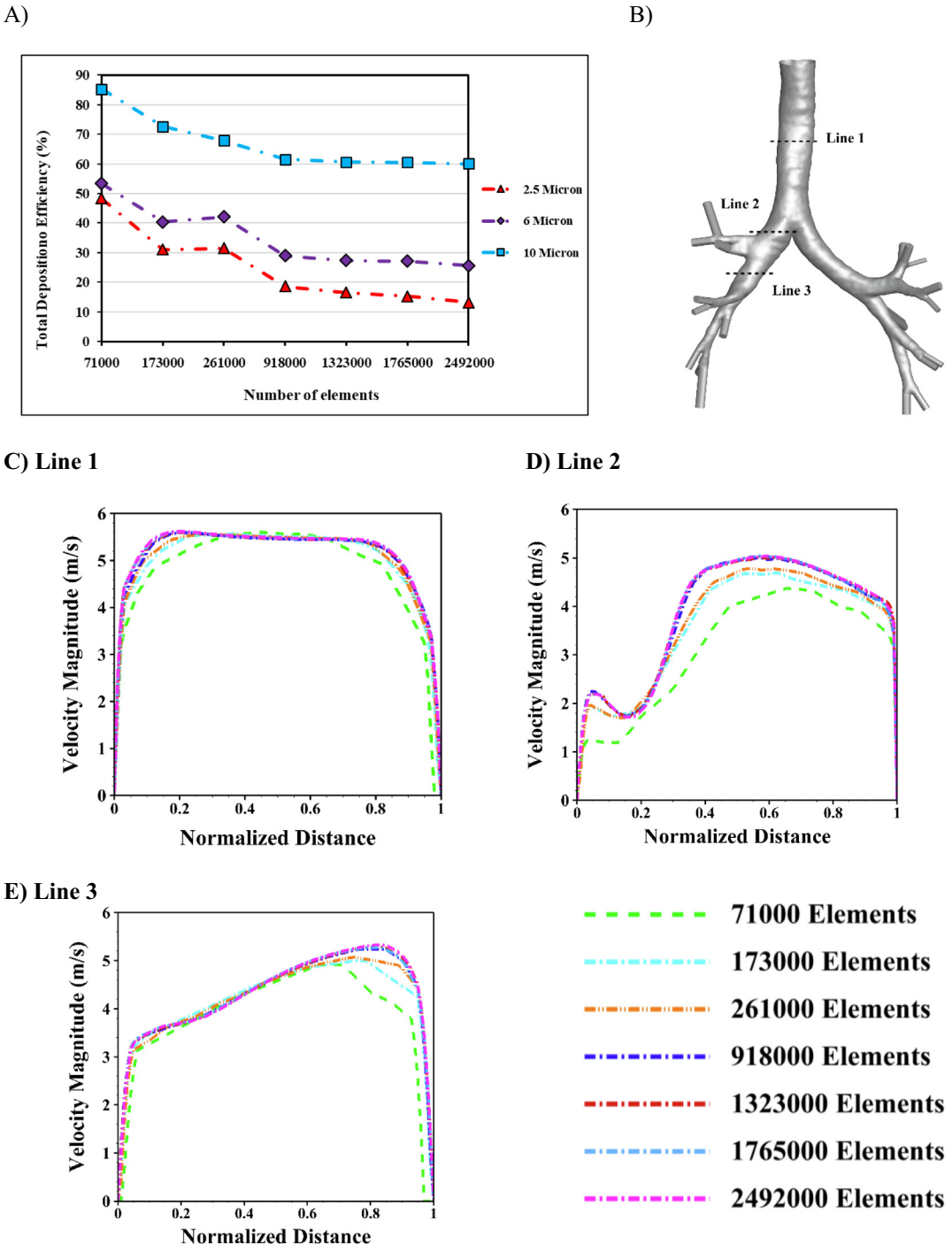

Fig. 5. Grid refinement results based on the total deposition of particles and velocity profiles at three distinct cross sections of the airways. A: Total deposition efficiency in the whole model of the respiratory airways. B: Position of the lines used for velocity profiles. C, D, E: Velocity profiles for different grid numbers on line 1, 2 and 3 respectively.

in ICEM in which the refinement algorithms have been applied to further enhance quality of the final mesh. The final mesh selected for simulations had an average quality of 0.86 which is rather enough for computational fluid dynamics simulations.

3. Results and discussion

3.1. Validation

In this study, a comprehensive analysis has been carried out to verify validity of the numerical method employed. The results of particle deposition in mouth throat model have been validated with a wide variety of previous studies reported in the literature [48,49,58–61,50–57].

Fig. 6 demonstrates deposition efficiency of particles against impaction parameter and compares the present numerical results with the numerical and experimental results presented in the literature. As there are different parameters that affect particle deposition, impaction parameter is introduced which accounts for both particle diameter and flow rate of the continuous phase and is proper for making comparison between the works that have used different particle diameter and flow rates. Fig. 6 demonstrates a broad spectrum of deposition results in the mouth throat region

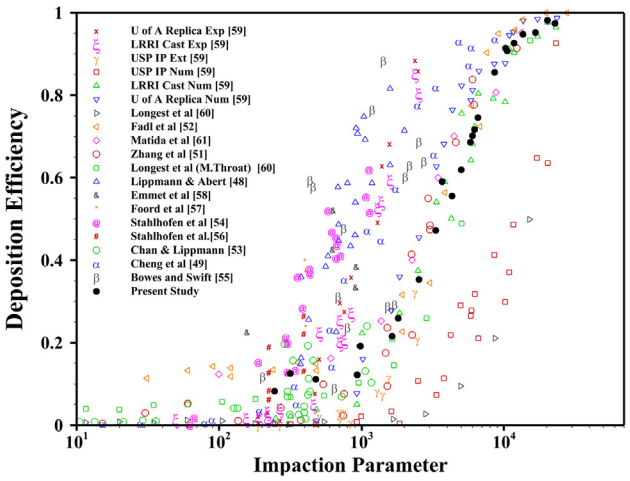

Fig. 6. Comparison of particle deposition in mouth throat model against impaction parameter with the numerical and experimental data presented in the literature.

obtained in different investigations. This deviation is due to the different geometrical details in each individual mouth-throat model and there are also other parameters involved such as the experimental conditions of each study and different numerical methods employed. However, it is observed in Fig. 6 that the results of the present numerical method fit properly among the available data depicted in Fig. 6 and indicates the validity of present numerical method.

3.2. Flow field analysis

The respiratory airways, particularly the lower respiratory system is very complex and can significantly influence the flow characteristics. The complex morphological geometry of the airways and local deflections in the flow path along with consecutive bifurcations drastically affect the flow streamlines and result in multiple regions of flow separation and secondary flows and diminish the symmetry of the flow. These factors all together alternate the local particle deposition patterns in different regions and hence, it is important to study the flow patterns and its characteristics in different regions of the respiratory system. Fig. 7 demonstrates the velocity profiles on different cross sections for the flow rate of 60 lpm. The positions of the planes have been shown schematically and the front (F) and rear (R) sides of the model have been marked in the figure. According to the velocity profiles depicted on the lines A and B which are in the main trachea, a more uniform distribution of momentum is observed while at higher generations, the velocity profiles are less uniform which is due to more complex geometry of airways and the separation of flow and secondary vortices generated. The velocity profiles presented in this figure are compatible with the contours of velocity magnitude which have been presented in Fig. 8. The velocity magnitude contours have been depicted in different transverse cross sections at different branches including the main trachea and other generations as well. These planes start from the trachea and encompass other bifurcations and branches in both the right and left lungs. The contours present the velocity and flow streamlines in three flow rates of 15, 30 and 60 L/min. It is observed that even small geometrical deflections affect the streamlines and secondary vortices are generated. This is observed in plane A where a vortex is generated at the rear side of the plane as a result of deflection which is due to presence of cartilage rings at the upper side of the trachea. The presence of secondary vortices is also observed in other regions due to sudden change in the flow path and numerous deflections in the geometry of the airways. In the first bifurcation, the flow divides into two main parts but as the left main stem bronchus is a little tighter than the right one, the flow accelerates due to continuity principle. This is indicated on the planes C and F. Another feature observed in Fig. 7 is that increasing the flow rates may diminish the vortices that are caused by separation. This incident is observed on planes F, G and H. In plane H and G, two vortices are observed in the flow rate of 15 lpm. As the flow rate increases, one of the vortices which is smaller vanishes and only one secondary vortices remain in the flow.

3.3. Distribution pattern

One of the most important reasons for studying aerosol transport in the respiratory system is the targeted delivery of pharmaceutical aerosols to desired locations. As inhaled particulates are used for pulmonary system treatment, it is important to recognize the distribution pattern of particles and know that how particles of different diameters distribute among different parts of the respiratory airways and which regions are more exposed to aerosols. The distribution fraction introduced in this section is the ratio of number of particles that have entered a specific region to the total number of particles that have been injected into the domain. It is derived by dividing the number of particles that have entered that region (which may have been deposited on the walls of that region or escaped through the outlet toward the lower generations) to the total number of particles that have been injected in the domain. Fig. 9A,B and c show the distribution fraction of particles for different lobes of the right and left lungs. Fig. 9 reveals that the greatest amount of particles are delivered to the right upper lobe, left lower lobe and right lower lobe respectively and right middle lobe receives the least amount of particles. This outcome is regarded to be important in case it is intended to deliver pharmaceutical particles to a desired location in the lungs. Another finding from this figure is that particle size and flow rate significantly influence delivery of drugs to different locations. According to Fig. 9, the amount of particles delivered to different lobes reduces by increasing the particle size and flow rate and this occurrence is particularly more remarkable about the upper lobes at right and left lungs. As it is indicated, the amount of particles delivered to the upper lobes in both the right and left lungs is significantly reduced for the particles with 14-μm diameter at flow rate of 60 L/min. This means that higher flow rates and larger particles should be avoided when it is intended to deliver the drugs to upper lobes in both lungs. On the other hand, the right middle lobe which receives the least amount of particles doesn't meet any considerable change by changing flow rate or particle size. To explain this finding, stokes number which is a dimensionless parameter can be illustrative. Stokes number is a dimensionless parameter that describes the flow of a particle in fluid flow. Stokes number is ratio of particle relaxation time to the characteristic time scale of the fluid flow and is expressed as:

$$st = \frac{\tau_D}{t_s} \tag{6}$$

Where

$$\tau_D = \frac{\rho_p {d_p}^2}{18\mu} \tag{7}$$

And

$$t_s = \frac{L_s}{V_s} \tag{8}$$

where τ_D is response time of particle, t_s is fluid response time, ρ_p is the particle density, d_p is particle diameter, μ is the fluid viscosity, L_s is characteristic length associated with the fluid flow and

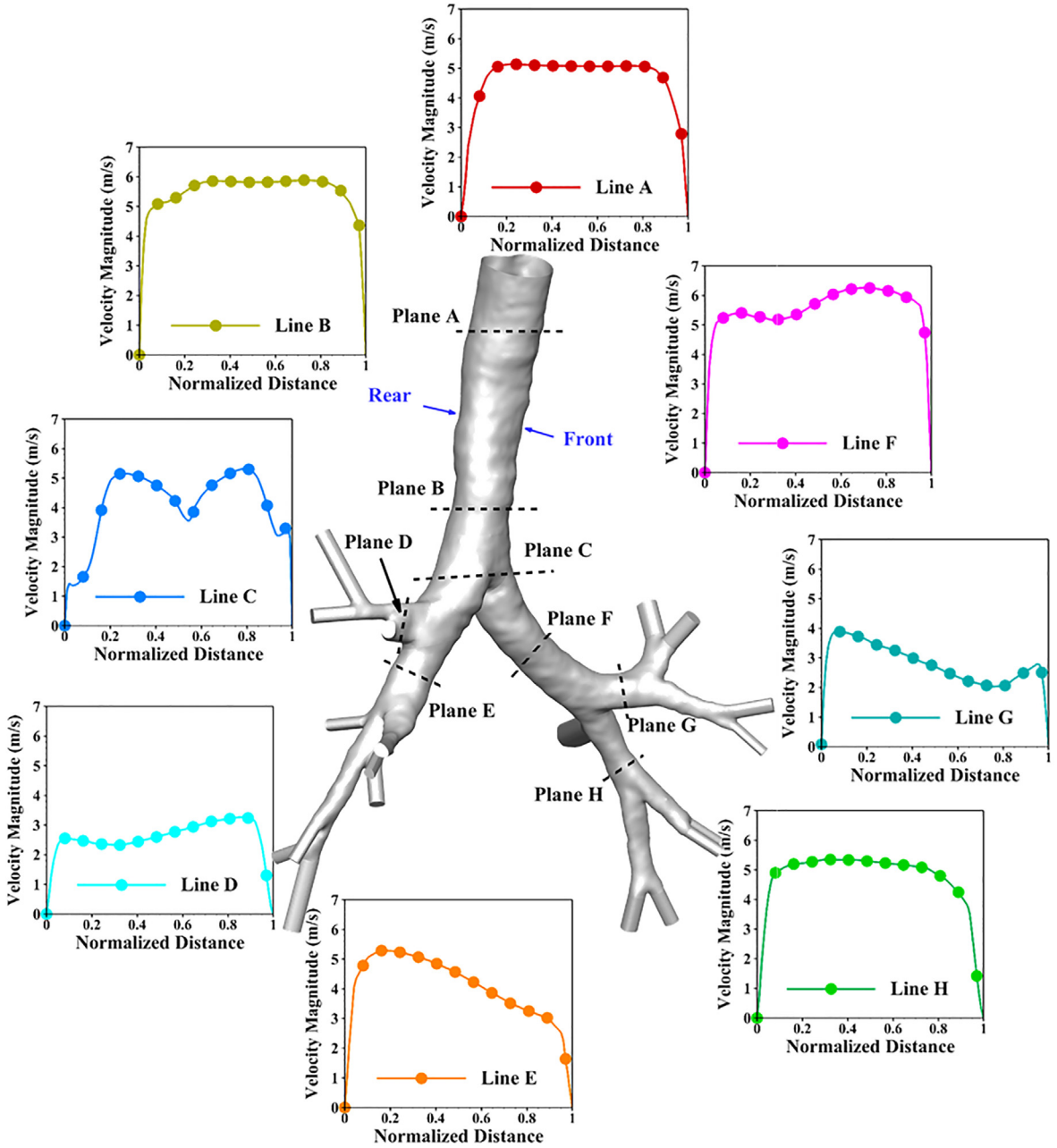

Fig. 7. Velocity profiles at different cross sections in the model including the trachea and lower generations for flow rate of 60 lpm. Positions of the planes and lines have been demonstrated on the model.

V_s is characteristic velocity of the fluid. Stokes number is an indication that how well can the particles follow the fluid flow streamlines. Lower stokes number means the particles can properly response to the flow streamlines and if a change in the flow path occurs, they can efficiently follow the flow path while higher stokes number means the response time of particles is greater than the response time of the system and particles may not follow the fluid flow properly. It is evident that the upper lobes in both right and left lungs deviate considerably from the main branch of the airways and the flow path changes a bit more toward the upper lobes. As stokes number is proportionate to both the flow velocity and particle size, increasing the flow rate and particle size increases the stokes number and hence, the particles cannot lean their path toward the upper lobes for higher stokes numbers. This phenomenon is apparently observed in Fig. 9C which is for flow rate of 60 lpm, where the distribution fraction of particles for the right and left upper lobes is significantly affected by increasing particle size and there is a remarkable reduction in the amount of particles that enter the right and left upper lobes. Analyzing how the particles may distribute among different lobes can give a better insight toward the use of pharmaceutical particulates for targeted drug delivery and may enhance the quality of diseases treatment.

Fig. 10 provides a better visualization of this phenomenon. Fig. 10A,B depict the distribution of particles in the domain 0.175 s after the injection for the 1-μm and 14-μm particles in the flow rate of 60 lpm. It is obviously seen that the particles with dp = 1 μm disperse more uniformly in different regions and the upper lobes in both the right and left lungs and they have almost occupied all the respiratory airways. As the diameter of particles

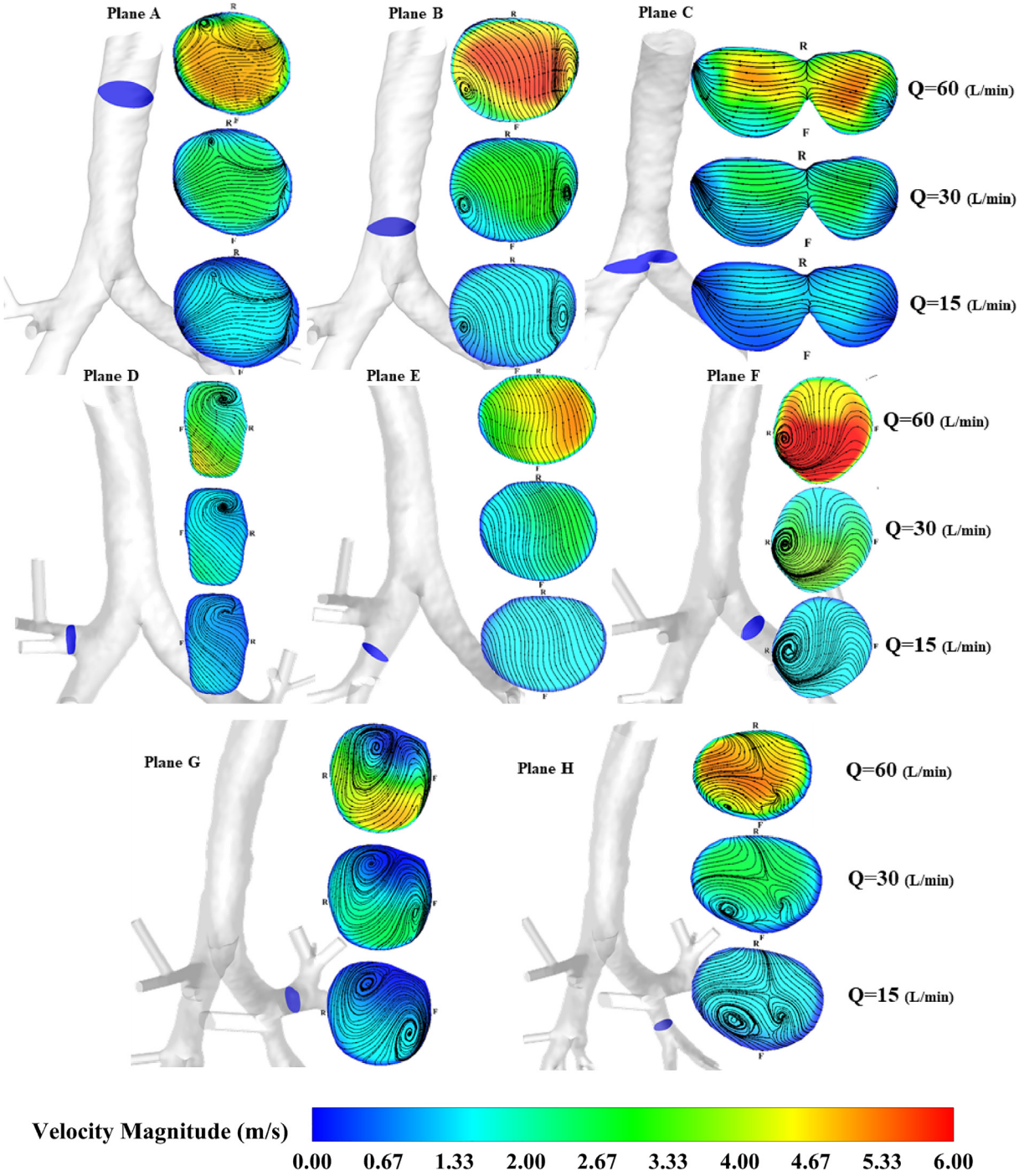

Fig. 8. Velocity magnitude contours and streamlines at different cross sections for flow rates of 15, 30 and 60 lpm. The positions of the planes have been marked with blue on the model. (For interpretation of the references to colour in this figure legend, the reader is referred to the web version of this article.)

increases (Fig. 10B), it is difficult for particles to bend their path with the flow stream and the distribution of particles is seen to be more oriented toward the regions with less deviation from the main path of the flow, as a result, less particles enter the upper lobes in both the right and left lungs. This is the reason than few number of particles are observed in the upper lobes in Fig. 10B.

Fig. 11 compares distribution of particles in the right and left lungs for different particle size at flow rate of 60 lpm. Fig. 11 indicates that the particles do not distribute equally between two lungs and majority of particles are delivered to the right lung. For 1-μm particles, 53.2% of the total particles injected into domain enter the right lung and 43.6% enter the left lung. This could be due to higher flow rate of the right lung in comparison with the left lung as stated in the work of Islam et al. [62]. However, as the particle size increases, the deposition rate of particles increases in the trachea and carina and as a result fewer number of particles remain in the domain. Consequently, the number of particles that distribute to each lung reduces with increasing the particle diameter as shown in Fig. 11.

3.4. Regional deposition

For an effective treatment, the pharmaceutics should deposit on desired regions which is why it is of great importance to have

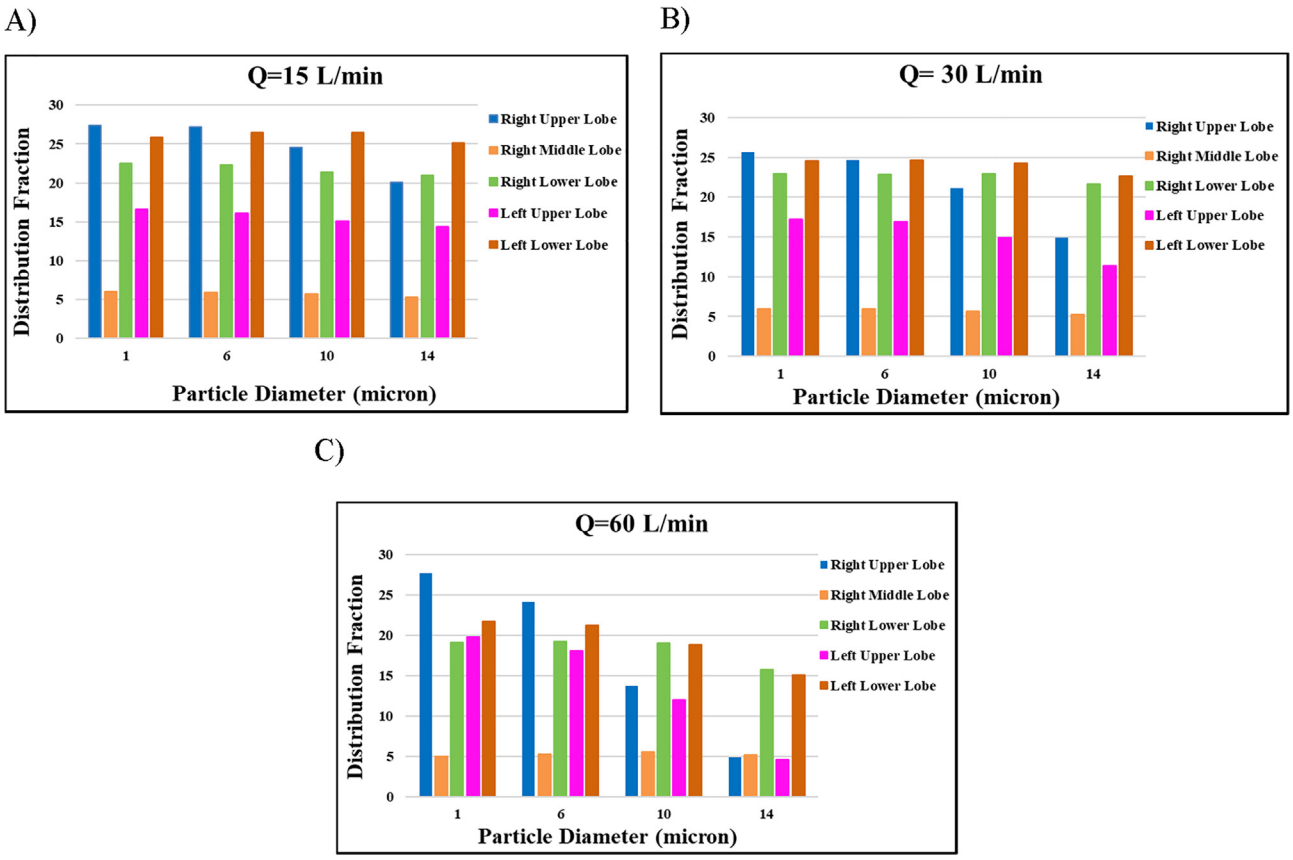

Fig. 9. Distribution fraction of particles in different lobes of the right and left lungs for particles with different sizes. A: Q = 15 L/min, B: Q = 30 L/min, C: Q = 60 L/min.

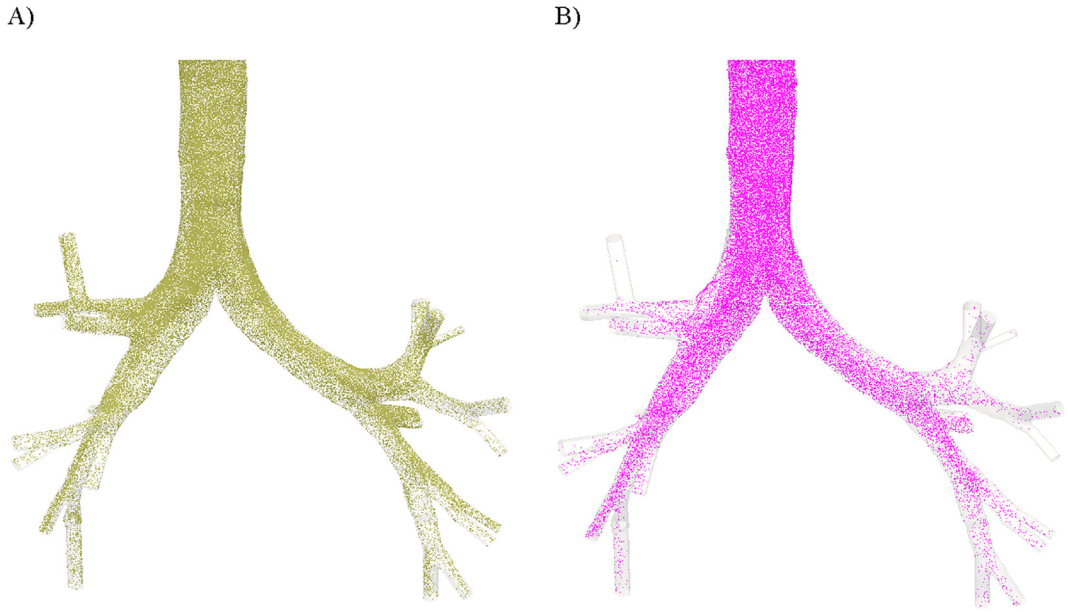

Fig. 10. distribution of particles in the respiratory airways 0.175 s after start of the injection for flow rate of 60 lpm. A) dp = 1 μm, B) and dp = 14 μm.

information about the deposition efficiencies at different regions of the pulmonary system. These data are especially beneficial in case of using pharmaceutical aerosols for disease cure in medical applications. It is also important for evaluating high risk regions in case of being exposed to polluted air with suspended aerosols. Fig. 12 makes a comparison of deposition of particles with 1, 6 and 14 μm in the right and left lungs in different flow rates. Fig. 12 indicates that at lower flow rates, the deposition in both lungs is rather equal for particles with different size but as the flow rate increases, the deposition in left lung exceeds the right lung. One main reason for this is the higher deviation of the left main stem bronchus from vertical line which causes excessive number of particles get depos-

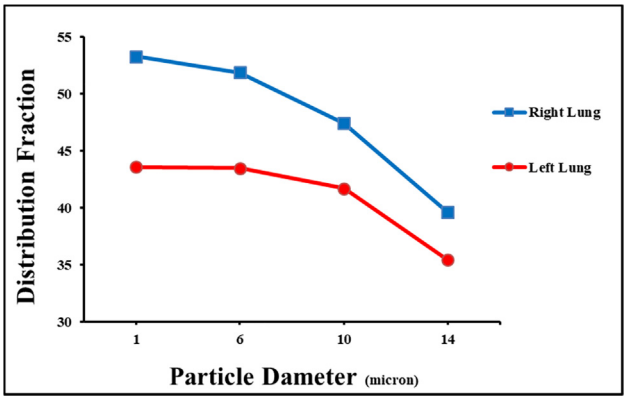

Fig. 11. Distribution fraction of particles in the right and left lungs for different particle sizes.

ited on it when the flow rate and particle diameter increases. As shown in Fig. 13C, there is an intense raise in the deposition of particles larger than 10 μm on the left main stem bronchus.

Fig. 13 A,B,C represent the deposition efficiency of particles with different diameter in the flow rates of 15, 30 and 60 lpm respectively. It is observed that in all flow rates, the left lower lobe bronchus and left main stem bronchus are two regions with highest rate of deposition for most of the particle sizes. On the contrary, the right main stem bronchus and right middle lobe bronchus are two regions with the least amount of particle deposition. It is also observed that deposition of particles increases with increase in the particles diameter and flow rate and it occurs remarkably for particles larger than 8-μm. This could be justified through considering inertial impaction which happens when particles can't follow the flow streamlines as a reason of high inertia and deposit on the surface of the wall. Any changes in the flow direction can enhance effect of inertial impaction. However, it is observed that at the flow rate of 60 lpm the particle deposition reduces at some regions for particles larger than 8 μm. This is result of filtration effect that takes place at the flow upstream. In other words, most of larger particles deposit on the walls at the initial generations of respiratory airways as a reason of inertial impaction which is due to incapability of larger particles to change their direction with flow stream. Accordingly, fewer particles find their way toward the lower generations which is why deposition efficiency reduces in these regions. This trend can be seen for flow rate of 60 lpm because higher flow rate intensifies effect of inertial impaction. As an instance, at flow rate of 60 lpm for particles larger than 10 μm, deposition efficiency reduces at the left upper lobe and left lower lobe which is because the deposition efficiency raises rapidly on the carina and left main stem bronchus. As a result, fewer particles remain for other regions in the left lung. The same is true about right upper lobe. Despite the filtration effect, it was previously mentioned that at higher flow rates, larger particles cannot find their path to the upper lobes and fewer particles enter that region which is why deposition reduces remarkably in the right upper lobe for flow rate of 60 lpm.

Fig. 14 depicts the deposition patterns for particles with 1 and 14 μm at flow rate of 60 lpm and can provide a better insight about the regions that are most prone to absorbing particles. As indicated in this figure, by increasing the size of particles, more particles get trapped on the initial bifurcations such as the main stem bronchi particularly at the left lung. As the flow rate and particle diameter increase (which both increase the stokes number), the inertial impaction plays the dominant role as a deposition mechanism which is why the main stem bronchi, carina and the bifurcations are the regions with most particle deposition. In Fig. 14B which is for the particles with 14 μm, main hotspots for deposition could be distinguished however, in Fig. 14A which is for 1 μm particles, a more uniform deposition pattern can be observed despite of the few number of particles that have been deposited. The left main stem bronchus is shown to receive a considerable amount of parti-

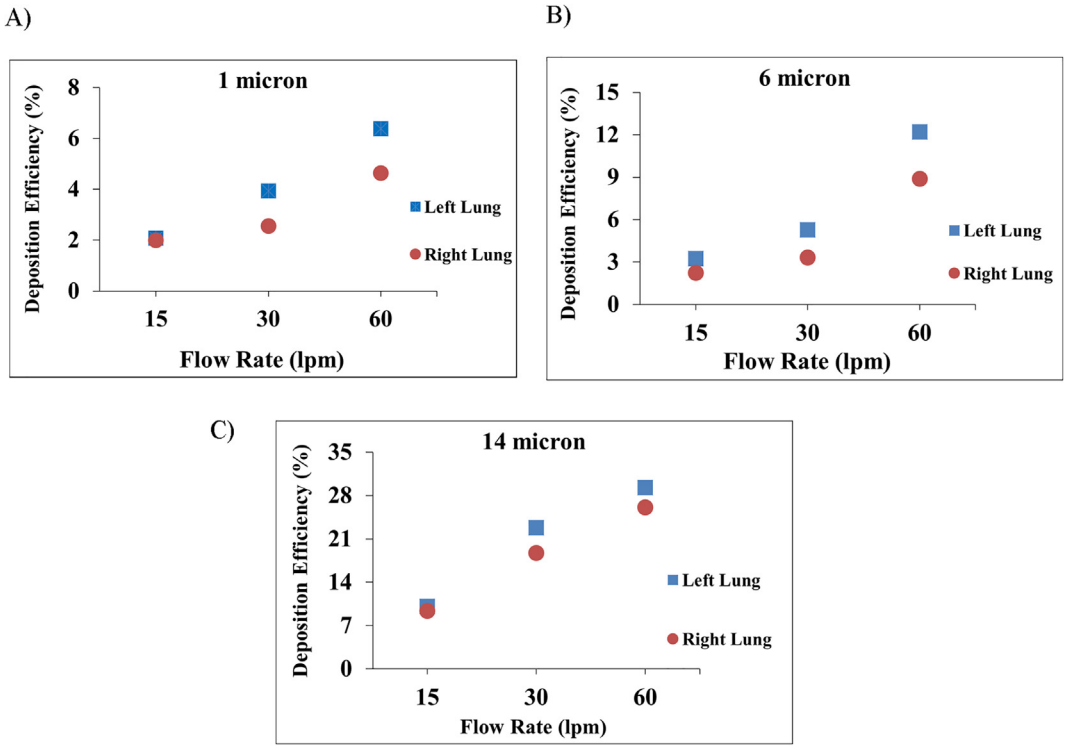

Fig. 12. Comparison of deposition efficiencies in the right and left lungs for particles with different diameter at different flow rates. A: 1 μm, B: 6 μm, C: 14 μm.

A)

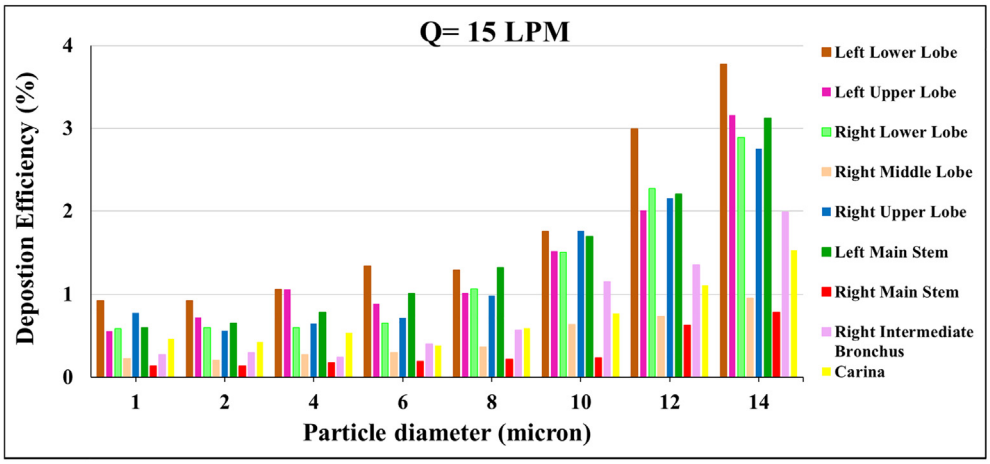

B)

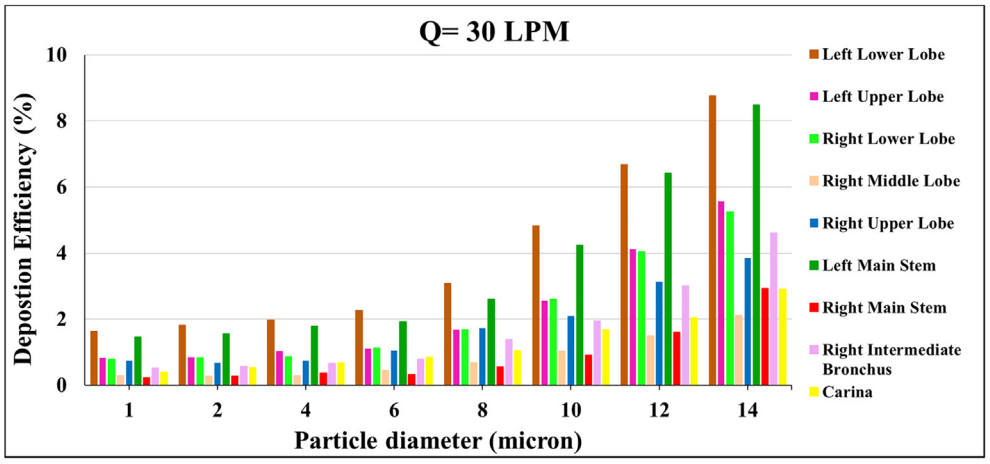

C)

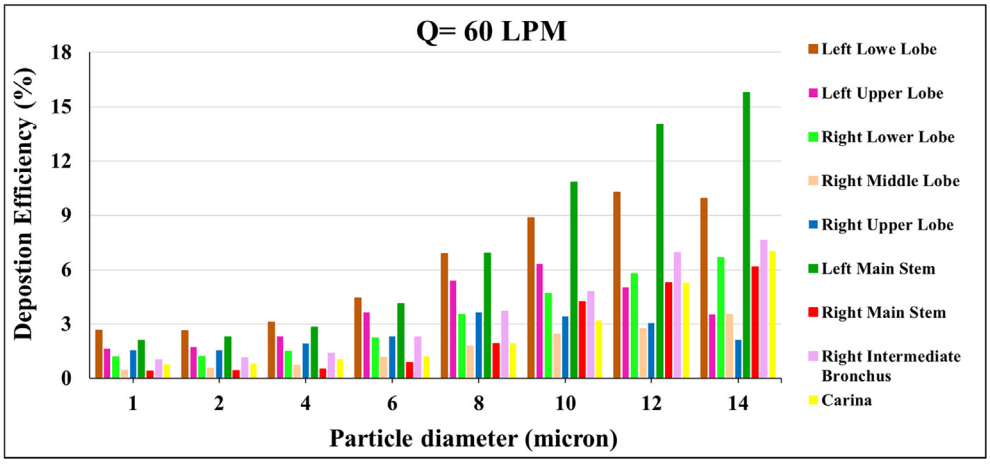

Fig.13. Lobar deposition for particles with different diameters at different flow rates (the colors for each lobe has been selected based on the colors indicated in Fig. 3 to better distinguish each region. A: 15 lpm, B: 30 lpm, C: 60 lpm.

cles in Fig. 14B This finding is compatible with Fig. 13. It could be elucidated by taking into account the geometrical shape of the primary bronchi. As shown in Fig. 3, geometry of two lungs is highly asymmetric and the left primary bronchus is more horizontally oriented and is longer than the right one which forces the flow to deviate from its initial path in the trachea. As a consequence, there is a higher rate of deposition in this region. This explains the progressive growth in deposition efficiency of the left and right main stem bronchi for larger particles in Fig. 13. As previously discussed, smaller particles with low inertia can be carried to lower genera-

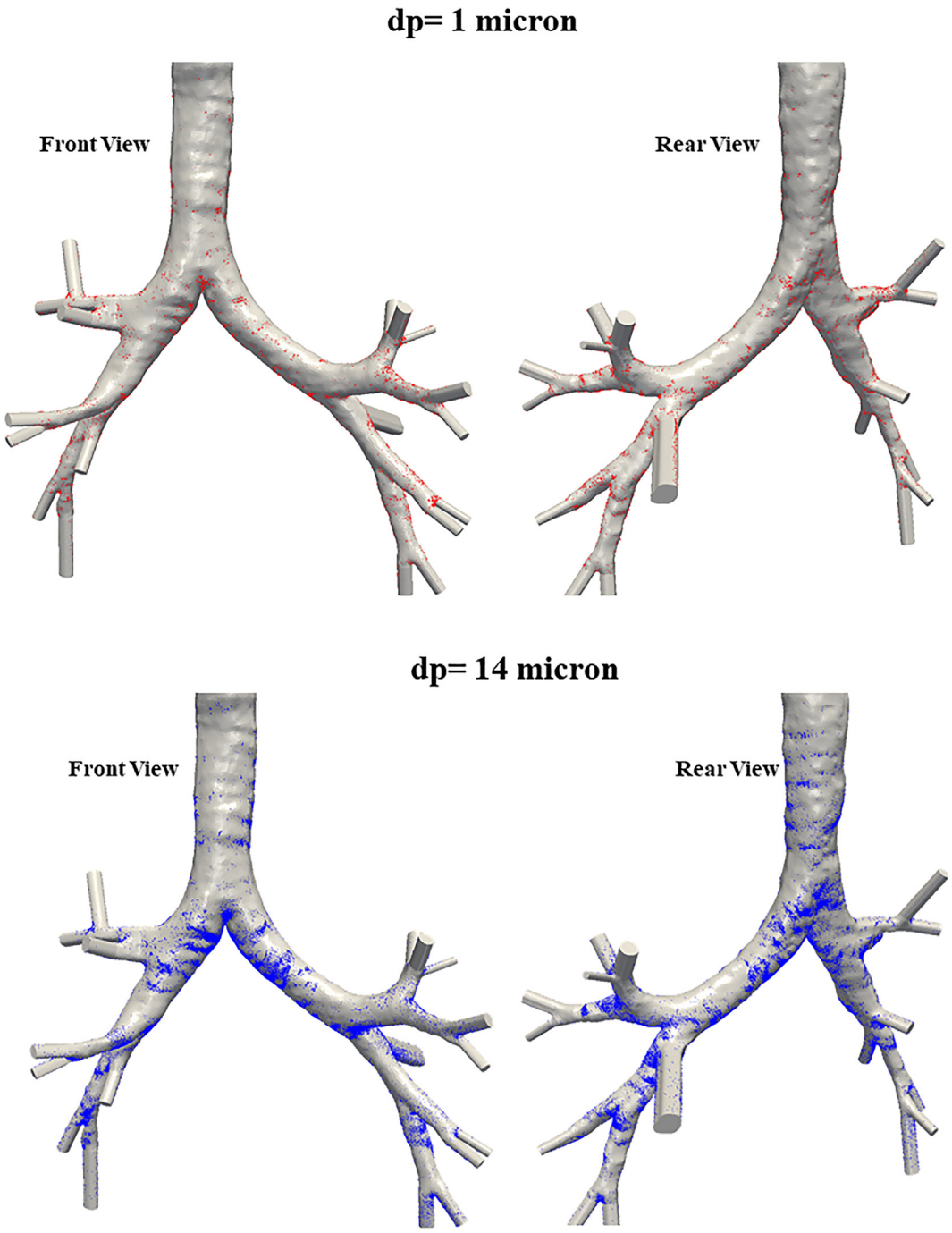

Fig. 14. Deposition patterns at flow rate of 60 lpm for 1 and 14 μm particles: both the front and rear views have been demonstrated.

tions of the airways by fluid flow and have inconsiderable deposition rate in the upper generations and most of them escape through the outlets of the model and move toward the lower generations.

4. Conclusion

In this study, flow field and distribution and deposition of particles with different diameters have been studied numerically in a realistic model of respiratory airways from the trachea to the end of segmental bronchi. The analysis has been performed for three flow rates of 15, 30 and 60 lpm which are associated with sedentary, light and heavy breathing conditions. To assess accuracy of the numerical method, a comprehensive validation has been carried out according to the numerical and experimental results presented in the literature. Geometrical characteristics of the model including the hydraulic diameter and perimeter at various transverse cross sections have been presented. In order to better understand flow characteristic, velocity magnitude contours and flow streamlines have been depicted on different cross sections of the model in different regions along with the velocity profiles as well. Despite the flow analysis, two-phase fluid-particle flow has also been analyzed and distribution and deposition patterns of particles have been studied to recognize the high risk regions that are more prone to absorb particles. The main results presented in this study are as follows:

- Morphological characteristics of the present patient specific model has been presented which includes the hydraulic diameter and perimeter of different transverse cross sections which encompass all the regions of the respiratory airways.
- At higher generations, the velocity profiles are less uniform which is due to complexity of the respiratory airways and flow separation and secondary vortices generated.
- The velocity contours and streamlines imply that even small geometrical deflections affect the streamlines and result in generation of secondary vortices. It was also observed that increasing flow rates may diminish the secondary vortices induced by separation.
- Majority of particles distribute to the right lung while deposition efficiency is higher in the left lung.
- Increasing particles size and flow rate increase the stokes number which is an indicator of response of the particle to the change in system parameters. As stokes number increases, the particles can barely adjust their direction with the flow path and more easily deposit on the initial generations of airways. This deposition mechanism is called inertial impaction.
- Increase in stokes number significantly influences the regions with higher deviation such as the left and right upper lobes and fewer particles enter these regions at higher flow rates for larger particles.
- The left lower lobe, left upper lobe and right lower lobe are the regions with highest rate of particle deposition.
- The filtration effect which occurs for particles with higher stokes number increases the deposition at initial generations and reduces the deposition efficiency in other regions.

Funding

This research did not receive any specific grant from funding agencies in the public, commercial, or not-for-profit sectors.

Declaration of Competing Interest

The authors declare that they have no known competing financial interests or personal relationships that could have appeared to influence the work reported in this paper.

References

[1] M. Rahimi-Gorji, L. Van de Sande, C. Debbaut, G. Ghorbaniasl, H. Braet, S. Cosyns, K. Remaut, W. Willaert, W. Ceelen, Intraperitoneal aerosolized drug delivery: Technology, recent developments, and future outlook, Adv. Drug Deliv. Rev. 160 (2020) 105–114, https://doi.org/10.1016/j.addr.2020.10.015.
[2] M.R. Gorji, C. Debbaut, G. Ghorbaniasl, W. Willaert, S. Cosyns, W. Ceelen, Electrostatic precipitation pressurized intraperitoneal aerosol chemotherapy (ePIPAC): Finding the optimal electrical potential, Eur. J. Surg. Oncol. 47 (2021) e30, https://doi.org/10.1016/j.ejso.2020.11.222.
[3] M. Hendryx, M.S. Islam, G.H. Dong, G. Paul, Air pollution emissions 2008–2018 from Australian coal mining: Implications for public and occupational health, Int. J. Environ. Res. Public Health 17 (2020), https://doi.org/10.3390/ijerph17051570.
[4] M. Rahimi-Gorji, C. Debbaut, G. Ghorbaniasl, S. Cosyns, W. Willaert, W. Ceelen, Optimization of intraperitoneal aerosolized drug delivery using computational fluid dynamics (CFD) modeling, Sci. Rep. 12 (2022) 6305, https://doi.org/10.1038/s41598-022-10369-8.
[5] M.S. Islam, P. Larpruenrudee, S.C. Saha, O. Pourmehran, A.R. Paul, T. Gemci, R. Collins, G. Paul, Y. Gu, How severe acute respiratory syndrome coronavirus-2 aerosol propagates through the age-specific upper airways, Phys. Fluids 33 (2021), https://doi.org/10.1063/5.0061627.
[6] M.S. Islam, S.C. Saha, T. Gemci, I.A. Yang, E. Sauret, Y.T. Gu, Polydisperse Microparticle Transport and Deposition to the Terminal Bronchioles in a Heterogeneous Vasculature Tree, Sci. Rep. 8 (2018) 1–9, https://doi.org/10.1038/s41598-018-34804-x.
[7] M.S. Islam, P. Larpruenrudee, S.I. Hossain, M. Rahimi-Gorji, Y. Gu, S.C. Saha, G. Paul, Polydisperse aerosol transport and deposition in upper airways of age-specific lung, Int. J. Environ. Res. Public Health 18 (2021), https://doi.org/10.3390/ijerph18126239.
[8] M.S. Islam, P. Larpruenrudee, A.R. Paul, G. Paul, T. Gemci, Y. Gu, S.C. Saha, SARS CoV-2 aerosol: How far it can travel to the lower airways?, Phys Fluids 33 (2021), https://doi.org/10.1063/5.0053351.
[9] M.S. Islam, S.C. Saha[1], E. Sauret, Y.T. Gu, Z.D. Ristovski, Numerical Investigation of Aerosol Particle Transport and Deposition in Realistic Lung Airway, in: Proceedings of the International Conference on Computational Methods, 2015.
[10] M.S. Islam, S.C. Saha, E. Sauret, H. Ong, P. Young, Y. Gu, Euler–Lagrange approach to investigate respiratory anatomical shape effects on aerosol particle transport and deposition, Toxicology Research and Application. 3 (2019) 239784731989467. https://doi.org/10.1177/2397847319894675.
[11] M.S. Islam, S.C. Saha, T. Gemci, I.A. Yang, E. Sauret, Z. Ristovski, Y.T. Gu, Euler-Lagrange Prediction of Diesel-Exhaust Polydisperse Particle Transport and Deposition in Lung: Anatomy and Turbulence Effects, Sci. Rep. 9 (2019) 1–16, https://doi.org/10.1038/s41598-019-48753-6.
[12] Q. Gu, S. Qi, Y. Yue, J. Shen, B. Zhang, W. Sun, W. Qian, M.S. Islam, S.C. Saha, J. Wu, Structural and functional alterations of the tracheobronchial tree after left upper pulmonary lobectomy for lung cancer, Biomed. Eng. Online 18 (2019) 1–18, https://doi.org/10.1186/s12938-019-0722-6.
[13] A. Ghosh, M.S. Islam, S.C. Saha, Targeted drug delivery of magnetic nanoparticle in the specific lung region, Computation. 8 (2020), https://doi.org/10.3390/computation8010010.
[14] P. Singh, V. Raghav, V. Padhmashali, G. Paul, M.S. Islam, S.C. Saha, Airflow and particle transport prediction through stenosis airways, Int. J. Environ. Res. Public Health 17 (2020), https://doi.org/10.3390/ijerph17031119.
[15] R. Mead-Hunter, A.J.C. King, A.N. Larcombe, B.J. Mullins, The influence of moving walls on respiratory aerosol deposition modelling, J. Aerosol Sci. 64 (2013) 48–59, https://doi.org/10.1016/j.jaerosci.2013.05.006.
[16] B. Sul, A. Wallqvist, M.J. Morris, J. Reifman, V. Rakesh, A computational study of the respiratory airflow characteristics in normal and obstructed human airways, Comput. Biol. Med. 52 (2014) 130–143, https://doi.org/10.1016/j.compbiomed.2014.06.008.
[17] X. Chen, W. Zhong, B. Sun, B. Jin, X. Zhou, Study on gas/solid flow in an obstructed pulmonary airway with transient flow based on CFD–DPM approach, Powder Technol. 217 (2012) 252–260.
[18] P.G. Koullapis, S.C. Kassinos, M.P. Bivolarova, A.K. Melikov, Particle deposition in a realistic geometry of the human conducting airways: Effects of inlet velocity profile, inhalation flowrate and electrostatic charge, J. Biomech. 49 (2016) 2201–2212, https://doi.org/10.1016/j.jbiomech.2015.11.029.
[19] O. Pourmehran, M. Rahimi-Gorji, M. Gorji-Bandpy, T.B. Gorji, Simulation of magnetic drug targeting through tracheobronchial airways in the presence of an external non-uniform magnetic field using Lagrangian magnetic particle tracking, J. Magn. Magn. Mater. 393 (2015) 380–393, https://doi.org/10.1016/j.jmmm.2015.05.086.
[20] J. Zhao, A. Haghnegahdar, Y. Feng, A. Patil, N. Kulkarni, G.J.P. Singh, G. Malhotra, R. Bharadwaj, Prediction of the carrier shape effect on particle transport, interaction and deposition in two dry powder inhalers and a mouth-to-G13 human respiratory system: A CFD-DEM study, J. Aerosol Sci. 160 (2022) 105899, https://doi.org/10.1016/j.jaerosci.2021.105899.
[21] M. Rahimi-Gorji, O. Pourmehran, M. Gorji-Bandpy, T.B. Gorji, CFD simulation of airflow behavior and particle transport and deposition in different breathing conditions through the realistic model of human airways, J. Mol. Liq. 209 (2015) 121–133, https://doi.org/10.1016/j.molliq.2015.05.031.
[22] N.L. Phuong, M. Yamashita, S.J. Yoo, K. Ito, Prediction of convective heat transfer coefficient of human upper and lower airway surfaces in steady and unsteady breathing conditions, Build. Environ. 100 (2016) 172–185, https://doi.org/10.1016/j.buildenv.2016.02.020.
[23] J.K. Narayanan, J. Lin, Y. Feng, X. Cui, Numerical study on the impact of mucus layer and inlet air-temperatures on the particle deposition in a highly idealized mouth-throat model using LES, Powder Technol. 395 (2022) 455–475, https://doi.org/10.1016/j.powtec.2021.09.073.
[24] B. Soni, S. Aliabadi, Computers & Fluids Large-scale CFD simulations of airflow and particle deposition in lung airway, Computers Fluids (2013), https://doi.org/10.1016/j.compfluid.2013.06.015.
[25] T. Deng, M.S.A. Bradley, Determination of a particle size distribution criterion for predicting dense phase pneumatic conveying behaviour of granular and powder materials, Powder Technol. (2016).
[26] X. Li, K. Inthavong, J. Tu, Particle inhalation and deposition in a human nasal cavity from the external surrounding environment, 47 (2011) 32–39. https://doi.org/10.1016/j.buildenv.2011.04.032.
[27] Y.D. Shang, K. Inthavong, J.Y. Tu, Detailed micro-particle deposition patterns in the human nasal cavity influenced by the breathing zone, Comput. Fluids 114 (2015) 141–150, https://doi.org/10.1016/j.compfluid.2015.02.020.
[28] P. Koullapis, S.C. Kassinos, J. Muela, C. Perez-Segarra, J. Rigola, O. Lehmkuhl, Y. Cui, M. Sommerfeld, J. Elcner, M. Jicha, I. Saveljic, N. Filipovic, F. Lizal, L. Nicolaou, Regional aerosol deposition in the human airways: The SimInhale benchmark case and a critical assessment of in silico methods, Eur. J. Pharm. Sci. (2017), https://doi.org/10.1016/j.ejps.2017.09.003.
[29] M.M. Rahman, M. Zhao, M.S. Islam, K. Dong, S.C. Saha, Aging effects on airflow distribution and micron-particle transport and deposition in a human lung using CFD-DPM approach, Adv. Powder Technol. 32 (2021) 3506–3516, https://doi.org/10.1016/j.apt.2021.08.003.
[30] M.M. Rahman, M. Zhao, M.S. Islam, K. Dong, S.C. Saha, Numerical study of nanoscale and microscale particle transport in realistic lung models with and without stenosis, Int. J. Multiph. Flow 145 (2021) 103842, https://doi.org/10.1016/j.ijmultiphaseflow.2021.103842.

[31] M. Sommerfeld, O.L. Sgrott, M.A. Taborda, P. Koullapis, K. Bauer, S. Kassinos, Analysis of flow field and turbulence predictions in a lung model applying RANS and implications for particle deposition, Eur. J. Pharm. Sci. 166 (2021) 105959, https://doi.org/10.1016/j.ejps.2021.105959.
[32] J. Williams, J. Kolehmainen, S. Cunningham, A. Ozel, U. Wolfram, Effect of patient inhalation profile and airway structure on drug deposition in image-based models with particle-particle interactions, Int. J. Pharm. 612 (2022) 121321, https://doi.org/10.1016/j.ijpharm.2021.121321.
[33] Y.H. Kim, D.D. Li, S. Park, D.S. Yi, G.H. Yeoh, A. Abbas, Computational investigation of particle penetration and deposition pattern in a realistic respiratory tract model from different types of dry powder inhalers, Int. J. Pharm. 612 (2022) 121293, https://doi.org/10.1016/j.ijpharm.2021.121293.
[34] W.H. Chen, C.M. Chang, J.K. Mutuku, S.S. Lam, W.J. Lee, Aerosol deposition and airflow dynamics in healthy and asthmatic human airways during inhalation, J. Hazard. Mater. 416 (2021) 125856, https://doi.org/10.1016/j.jhazmat.2021.125856.
[35] R. Tohidi, B. Sajadi, G. Ahmadi, The effect of nasal airway obstruction on the dispersion and deposition of inhaled volatile droplets in the human nasal cavity: A numerical study, J. Aerosol Sci. 150 (2020) 105650, https://doi.org/10.1016/j.jaerosci.2020.105650.
[36] W. Liu, Y. Wu, G. Liu, H. Lu, Study on the multi-component particle-gas two-phase flow in a human upper respiratory tract, Powder Technol. 397 (2022) 117030, https://doi.org/10.1016/j.powtec.2021.117030.
[37] C. Wu, W. Yan, R. Chen, Y. Liu, G. Li, Numerical study on targeted delivery of magnetic drug particles in realistic human lung, Powder Technol. 397 (2022) 116984, https://doi.org/10.1016/j.powtec.2021.11.028.
[38] C. Xu, X. Zheng, S. Shen, A numerical study of the effects of ambient temperature and humidity on the particle growth and deposition in the human airway, Environ. Res. 200 (2021) 111751, https://doi.org/10.1016/j.envres.2021.111751.
[39] N.A. Moore, W.A. Roy, Gross and Developmental Anatomy, Mosby/Elsevier (2010). https://books.google.com/books?id=_mcevuyZArAC.
[40] C.L. Lin, M.H. Tawhai, G. McLennan, E.A. Hoffman, Characteristics of the turbulent laryngeal jet and its effect on airflow in the human intra-thoracic airways, Respir. Physiol. Neurobiol. 157 (2007) 295–309, https://doi.org/10.1016/j.resp.2007.02.006.
[41] F.S. Stylianou, J. Sznitman, S.C. Kassinos, Direct numerical simulation of particle laden flow in a human airway bifurcation model, Int. J. Heat Fluid Flow 61 (2016) 677–710, https://doi.org/10.1016/j.ijheatfluidflow.2016.07.013.
[42] Fluent, ANSYS FLUENT User ' s Guide, 15317 (2011) 2498. http://cdlab2.fluid.tuwien.ac.at/LEHRE/TURB/Fluent.Inc/v140/flu_ug.pdf.
[43] Z. Zhang, C. Kleinstreuer, C.S. Kim, Cyclic micron-size particle inhalation and deposition in a triple bifurcation lung airway model, J. Aerosol Sci. 33 (2002) 257–281, https://doi.org/10.1016/S0021-8502(01)00170-7.
[44] M. Rahimi-Gorji, T.B. Gorji, M. Gorji-Bandpy, Details of regional particle deposition and airflow structures in a realistic model of human tracheobronchial airways: Two-phase flow simulation, Comput. Biol. Med. 74 (2016) 1–17, https://doi.org/10.1016/j.compbiomed.2016.04.017.
[45] J. Xi, P.W. Longest, Transport and deposition of micro-aerosols in realistic and simplified models of the oral airway, Ann. Biomed. Eng. 35 (2007) 560–581, https://doi.org/10.1007/s10439-006-9245-y.
[46] A. Gosman, E. Ioannides, Aspects of computer simulation of liquid-fuelled combustors, in: 19th Aerospace Sciences Meeting, American Institute of Aeronautics and Astronautics, 1981. https://doi.org/doi:10.2514/6.1981-323.
[47] S.A. Morsi, A.J. Alexander, An investigation of particle trajectories in two-phase flow systems, J. Fluid Mech. 55 (1972) 193, https://doi.org/10.1017/S0022112072001806.
[48] M. Lipmann, R.E. Albert, The Effect of Particle Size on the Regional Deposition of Inhaled Aerosols in the Human Respiratory Tract, Am. Ind. Hyg. Assoc. J. 30 (1969) 257–275, https://doi.org/10.1080/00028896909343120.
[49] Y.S. Cheng, Y. Zhou, B.T. Chen, Particle deposition in a cast of human oral airways, Aerosol Sci. Technol. 31 (1999) 286–300, https://doi.org/10.1080/027868299304165.
[50] A. Dehbi, Turbulent particle dispersion in arbitrary wall-bounded geometries: A coupled CFD-Langevin-equation based approach, Int. J. Multiph. Flow 34 (2008) 819–828, https://doi.org/10.1016/j.ijmultiphaseflow.2008.03.001.
[51] Z. Zhang, C. Kleinstreuer, C.S. Kim, Y.S. Cheng, Vaporizing Microdroplet Inhalation, Transport, and Deposition in a Human Upper Airway Model, Aerosol Sci. Technol. 38 (2004) 36–49, https://doi.org/10.1080/02786820490247597.
[52] A. Fadl, J. Wang, Z. Zhang, Y. Sung Cheng, Effects of MDI spray angle on aerosol penetration efficiency through an oral airway cast, J. Aerosol Sci. 38 (2007) 853–864, https://doi.org/10.1016/j.jaerosci.2007.06.002.
[53] T.L. Chan, M. Lippmann, Experimental measurements and empirical modelling of the regional deposition of inhaled particles in humans, Am. Ind. Hyg. Assoc. J. 41 (1980) 399–409, https://doi.org/10.1080/15298668091424942.
[54] W. Stahlhofen, J. Gebhart, J. Heyder, G. Scheuch, New Regional Deposition Data of the Human Respiratory Tract, J. Aerosol Sci. 14 (1983) 186–188, https://doi.org/10.1016/0021-8502(83)90022-8.
[55] S.M. Bowes, D.L. Swift, Deposition of inhaled particles in the oral airway during oronasal breathing, Aerosol Sci. Technol. 11 (1989) 157–167, https://doi.org/10.1080/02786828908959308.
[56] W. Stahlhofen, J. Gebhar, J. Heyder, Experimental determination of the regional deposition of aerosol particles in the human respiratory tract, Am. Ind. Hyg. Assoc. J. 40 (1980) 9–13.
[57] N. Foord, A. Black, M. Walsh, Regional deposition of 2.5-7.5 μm diameter inhaled particles in healthy male non-smokers, J. Aerosol Sci. 9 (1978) 343–357, https://doi.org/10.1016/0021-8502(78)90037-X.
[58] P.C. Emmett, R.J. Aitken, W.J. Hannan, Measurements of the total and regional deposition of inhaled particles in the human respiratory tract, J. Aerosol Sci. 13 (1982) 549–560, https://doi.org/10.1016/0021-8502(82)90020-9.
[59] Y. Zhou, J. Sun, Y.S. Cheng, Comparison of deposition in the USP and physical mouth-throat models with solid and liquid particles, Journal of Aerosol Medicine and Pulmonary, Drug Delivery 24 (2011) 277–284, https://doi.org/10.1089/jamp.2011.0882.
[60] P.W. Longest, M. Hindle, S. Das, J. Xi, Comparison of ambient and spray aerosol deposition in a standard induction port and more realistic mouth – throat geometry, J. Aerosol Sci. 39 (2008) 572–591, https://doi.org/10.1016/j.jaerosci.2008.03.008.
[61] E.A. Matida, W.H. Finlay, C.F. Lange, B. Grgic, Improved numerical simulation of aerosol deposition in an idealized mouth-throat, J. Aerosol Sci. 35 (2004) 1–19, https://doi.org/10.1016/S0021-8502(03)00381-1.
[62] M.S. Islam, S.C. Saha, E. Sauret, T. Gemci, Y.T. Gu, Pulmonary aerosol transport and deposition analysis in upper 17 generations of the human respiratory tract, J. Aerosol Sci. 108 (2017) 29–43, https://doi.org/10.1016/j.jaerosci.2017.03.004.